



NRC Publications Archive Archives des publications du CNRC

Influence of soot aggregate size and internal multiple scattering on LII signal and the absorption function variation with wavelength determined by the TEW-LII method

Yon, J.; Therssen, E.; Liu, F.; Bejaoui, S.; Hebert, D.

This publication could be one of several versions: author's original, accepted manuscript or the publisher's version. / La version de cette publication peut être l'une des suivantes : la version prépublication de l'auteur, la version acceptée du manuscrit ou la version de l'éditeur.

For the publisher's version, please access the DOI link below. / Pour consulter la version de l'éditeur, utilisez le lien DOI ci-dessous.

Publisher's version / Version de l'éditeur:

<https://doi.org/10.1007/s00340-015-6116-y>

Applied Physics B, 119, 4, pp. 643-655, 2015-05-07

NRC Publications Record / Notice d'Archives des publications de CNRC:

<https://nrc-publications.canada.ca/eng/view/object/?id=9ebb268a-3605-45fa-b8bc-e906d079e417>

<https://publications-cnrc.canada.ca/fra/voir/objet/?id=9ebb268a-3605-45fa-b8bc-e906d079e417>

Access and use of this website and the material on it are subject to the Terms and Conditions set forth at

<https://nrc-publications.canada.ca/eng/copyright>

READ THESE TERMS AND CONDITIONS CAREFULLY BEFORE USING THIS WEBSITE.

L'accès à ce site Web et l'utilisation de son contenu sont assujettis aux conditions présentées dans le site

<https://publications-cnrc.canada.ca/fra/droits>

LISEZ CES CONDITIONS ATTENTIVEMENT AVANT D'UTILISER CE SITE WEB.

Questions? Contact the NRC Publications Archive team at

PublicationsArchive-ArchivesPublications@nrc-cnrc.gc.ca. If you wish to email the authors directly, please see the first page of the publication for their contact information.

Vous avez des questions? Nous pouvons vous aider. Pour communiquer directement avec un auteur, consultez la première page de la revue dans laquelle son article a été publié afin de trouver ses coordonnées. Si vous n'arrivez pas à les repérer, communiquez avec nous à PublicationsArchive-ArchivesPublications@nrc-cnrc.gc.ca.



Influence of soot aggregate size and internal multiple scattering on LII signal and the absorption function variation with wavelength determined by the TEW-LII method

J. Yon¹ · E. Therssen² · F. Liu³ · S. Bejaoui² · D. Hebert¹

Received: 12 November 2014 / Accepted: 21 April 2015 / Published online: 7 May 2015
© Springer-Verlag Berlin Heidelberg 2015

Abstract Laser-induced incandescence (LII) is a powerful and robust optical method for in situ determination of soot volume fraction and/or soot absorption/emission properties in flames and engine exhaust. The laser-induced signal is interpreted as thermal emission based on the Planck law. Up to now, the evaluation and interpretation of LII signal have been largely based on contributions from isolated primary particles that are assumed much smaller than wavelengths. In the present paper, the morphology, wavelength, and aggregate size-dependent effects of multiple scattering within fractal soot aggregates on their absorption and emission cross sections are taken into account in the evaluation of LII signal by proposing correction terms to the traditional model. The impact of accounting for the correction to soot aggregate emission due to multiple scattering on LII signal and on the two excitation wavelength-induced incandescence method for inferring the soot absorption function, $E(m)$, is discussed. For wavelengths shorter than 532 nm, $E(m, \lambda)/E(m, 1064 \text{ nm})$ increases more significantly with decreasing wavelength. For wavelengths longer than 532 nm, the wavelength dependence of $E(m, \lambda)/E(m, 1064 \text{ nm})$ becomes very small and can be neglected. The proposed corrections, along with the soot morphology, are applied to re-analyze the experimental data of Bejaoui et al.

(Appl Phys B Lasers Opt, 116:313, 2014) for deriving the relative soot absorption function variation with wavelength at different locations in a rich premixed methane flat flame at atmospheric pressure. The present analysis showed that the soot absorption function varies with the height above the burner exit and can be correlated with the degree of soot maturation.

1 Introduction

Laser-induced incandescence (LII) is a laser based in situ technique that has been increasingly used to determine the volume fraction of soot particles. The principle of LII is to rapidly heat the nano-sized soot particles by thermally energizing them (using a pulsed laser beam of nano-second duration) to temperatures significantly higher than the temperature of the investigated medium and to measure the resulting incandescence signal interpreted as thermal emissions based on the Planck law. Since the discovery of the LII phenomenon [2, 3] and the recognition that it can be used as a soot diagnostics [4], LII has been developed into a powerful and versatile soot diagnostic technique and continuously improved. For example, the two-color LII technique (2C-LII), in which the incandescence signal is detected at two wavelengths in the visible spectrum, has been demonstrated to be superior to the conventional one-color LII technique, since it provides information of the particle temperature during the LII process and does not require calibration against a source of known particle concentration [5, 6]. The recent advances in LII modeling, in particular in the low-fluence regime and refinement in the soot properties, permit the in situ determination of primary particle size by analyzing the decay rate of LII signal or soot temperature through detection of time-resolved LII

✉ J. Yon
yon@coria.fr

¹ CORIA-UMR6614, Normandie Université, CNRS, INSA et Université de Rouen, Av de l'Université, 76801 Saint Etienne du Rouvray, France

² PC2A, UMR 8522 CNRS, Université Lille 1, 59655 Villeneuve d'Ascq, France

³ Black Carbon Metrology, Measurement Science and Standards, National Research Council, Ottawa, ON, Canada

signal [6]. The coupling of this technique with other ones, such as laser light scattering, permits to determine the particle volume fraction, primary particle, and aggregate sizes [7].

In most LII studies, the absorption and emission properties of soot particles are evaluated using the Rayleigh–Debye–Gans theory for fractal aggregates (RDG-FA). Using this theory, the LII signal is proportional to the product of the number of aggregates per unit volume (N_{agg}), the number of primary particle inside the aggregate (N_p), and to the absorption cross section of primary particle (σ_p). Because this theory assumes the primary particles are much smaller than the wavelength (Rayleigh regime), their absorption cross section becomes proportional to the product of the primary particle diameter D_p raised to the power of 3, the absorption function $E(m)$, which is a function of the soot refractive index, and the inverse of the wavelength of the laser source. As such, the LII signal is proportional to $N_{\text{agg}} \times N_p \times D_p^3 \times E(m)/\lambda$ that is directly proportional to the soot volume fraction. However, several studies, [8, 9], have shown that the aggregate absorption cross section is not exactly proportional to the product of N_p and σ_p . Indeed, the complex phenomena, namely the internal multiple scattering effects induced by the fractal-like morphology of the particle and for certain wavelengths non-strictly Rayleigh regime, can either reduce or enhance the absorption cross section from the one evaluated by the aforementioned method, depending on the aggregate size and wavelength.

The recent study [8] introduced a correction factor for the evaluation of the aggregate absorption cross section, which was determined by the discrete-dipole approximation (DDA) calculations for a wide range of aggregate size between $N_p = 1$ and 1006 (number of primary particles) and wavelength between 266 and 1064 nm and was found to fall between 0.6 and 1.3. The departure of the correction factor from unity reflects the effect of multiple scattering within the aggregate and is dependent on aggregate size and wavelength. The benefit of introducing this correction factor is to evaluate more accurately the aggregate absorption cross section at accuracy close to that of DDA while keeping the fairly simple analytical expression of the RDG-FA theory [10]. The first objective of the present paper is to propose a revised expression for the LII signal that incorporates the multiple scattering effects.

One of the main sources of uncertainty in soot measurements based on attenuation or emission is due to the uncertainty in the soot absorption function $E(m)$ in the visible spectrum. There seems a consensus in the literature that this value falls in the range of about 0.2–0.4, i.e., with a uncertainty of about a factor of 2. Nevertheless, investigations conducted so far tend to support that $E(m)$ seems dependent on the type of fuel and the maturation of the soot particle

[11–13]. It is well known that the soot absorption function is difficult to determine accurately and many methods have been proposed [12, 14–22]. Among these methods, the two excitation wavelength LII (TEW-LII) technique seeks to produce identical time-resolved and spectrally resolved LII signals by adjusting the laser pulse energy at two different laser wavelengths and permits to determine the relative spectral dependence of $E(m)$ [1]. The principle of TEW-LII to determine the relative $E(m)$ variation is to ensure that the soot particles under the two excitations are subject to the same amount of energy absorption from the laser pulse. It is an in situ method which is relatively simple to implement. This technique has been recently generalized to four pairs of wavelength [1] and shown that the relative spectral dependence of $E(m)$ seems independent of either the fuel type or the position in the flames investigated. As explained by Bejaoui et al. [1], these results are not in disagreement with previous studies showing an increase in the absorption function from nascent soot low in rich premixed flat flames to more mature soot (mainly composed of black carbon with an advanced graphitization state) in higher locations from the burner exit, since TEW-LII only provides the relative spectral dependence of $E(m)$, but not the absolute values. Nevertheless, similar to the theoretical expression for the LII signal, the theory of TEW-LII formulated so far has also neglected the multiple scattering effects on aggregate absorption/emission. Therefore, the second objective of the present paper is to re-analyze the TEW-LII results of Bejaoui et al. [1] by taking into account the multiple scattering effects on aggregate absorption cross section using the correction factor of Yon et al. [8].

The first part of the paper deals with the formulation of the LII signal with the multiple scattering effect and aggregate size distribution taken into account. The second part will discuss how accounting for these effects affects the interpretation of the spectral dependence of the $E(m)$ ratio determined using TEW-LII. Finally, the impact of those effects on the relative and absolute absorption function as a function of the position in a rich premixed flat flame will be presented.

2 Theory

2.1 Impact of aggregate morphology on LII signal

Let us consider the thermal emission coming from a small measurement volume ΔV containing isothermal and uniformly distributed soot particles characterized by its emissivity ε and temperature T . The measurement volume is formed with a cross-sectional area ΔS (related to the detection optics) and a thickness Δx (controlled by the laser beam size), i.e., $\Delta V = \Delta S \times \Delta x$. The radiative power

collected on a detector placed at a distance of D from the considered volume of measurement and normal to ΔS in the wavelength range $[\lambda_{\text{det}}, \lambda_{\text{det}} + d\lambda_{\text{det}}]$ is:

$$d\text{LII}(\lambda_{\text{det}}) = \varepsilon_{\lambda_{\text{det}}} \frac{\eta_{\lambda_{\text{det}}} L_{\lambda_{\text{det},T}}^{\circ}}{D^2} \Delta S d\lambda_{\text{det}} \quad (1)$$

where $L_{\lambda_{\text{det},T}}^{\circ}$ is the black body spectral radiance (the power emitted per unit area, per unit solid angle, and per unit wavelength interval following the Planck law) and $\eta_{\lambda_{\text{det}}}$ is the detector conversion factor depending on the wavelength. By the application of the Kirchoff law, the emissivity of this thin layer of soot aerosol is related to the absorption coefficient K_{abs} as follows

$$\varepsilon_{\lambda} = K_{\text{abs}}(\lambda) \Delta x \quad (2)$$

assuming the optical thickness $K_{\text{abs},\lambda} \Delta x$ is much less than 1. The LII signal can then be obtained as the integration over a narrow bandwidth $\Delta\lambda_{\text{det}}$ centered at the detection wavelength λ_{det} , i.e., $[\lambda_{\text{det}} - \Delta\lambda_{\text{det}}/2, \lambda_{\text{det}} + \Delta\lambda_{\text{det}}/2]$

$$\text{LII}(\lambda_{\text{det}}) = \frac{\Delta V C_1 \eta_{\lambda_{\text{det}}} K_{\text{abs}}(\lambda_{\text{det}})}{D^2} \frac{1}{\lambda_{\text{det}}^5} \left(\exp\left(\frac{C_2}{\lambda_{\text{det}} T}\right) - 1 \right)^{-1} \Delta\lambda_{\text{det}} \quad (3)$$

where $C_1 = 2\bar{h} \left(\frac{c_0}{n}\right)^2 \approx 1.1910^8 \text{ W m}^{-2} \mu\text{m}^{-4}$ and $C_2 = \frac{\bar{h} c_0}{k_B n} \approx 14400 \mu\text{m K}$.

Let us now consider the evaluation of the absorption coefficient of soot aggregates contained in the volume of measurement. The simplest analytical approach is to use the well-known RDG-FA theory [10, 23, 24]. This theory is formulated based on the following assumptions. First, primary spheres are in the Rayleigh limit, implying that the refractive index m and the primary sphere diameter D_p have to be such that the phase shift and the size parameters are small, i.e., $|m - 1| \ll 1$, $2\pi D_p |m - 1|/\lambda < 1$, and $\pi D_p/\lambda \ll 1$. Secondly, each primary sphere is exposed to the incident light, suggesting that the aggregate structure is sufficiently open with a fractal dimension < 2 ($D_f < 2$). Thirdly, the scattered intensity is considered as the summation of the intensities scattered by individual primary sphere, i.e., neglecting the multiple scattering within the aggregate. The first assumption has been found reasonably valid for soot aggregates in visible range [25]. Limitations of RDG-FA associated with the second and the third assumptions have been studied by comparing RDG-FA with more accurate numerical evaluations of the aggregate-light interaction [8, 9, 26] and the error of RDG-FA has been considered similar to experimental uncertainties [10, 27–29]. In essence, RDG-FA is the first-order theory with high-order effects neglected [10]. The RDG-FA theory states that aggregate absorption cross section is proportional to the absorption cross section of the primary particle $C_{\text{abs}}^{\text{mono}}$ and to the number of primary spheres in the

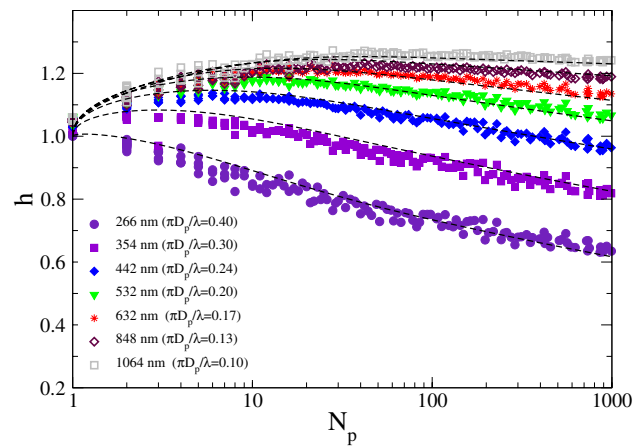


Fig. 1 Variation of the absorption correction factor h with the aggregate size and wavelength. These correction factors were calculated for DLCA aggregates formed by polydisperse primary particles with mean and variance of 34.2 and 6.85 nm, respectively (DLCA results adapted from [8])

aggregate N_p , i.e., the aggregate absorption cross section is not affected by aggregation and is independent of the fractal parameters. However, it has been well established that the aggregate absorption is indeed dependent on the morphology, such as N_p , fractal dimension D_f , and prefactor k_f , as well as wavelength, see [9] and some references cited therein. The fundamental reason for the dependence of aggregate absorption on morphology is the multiple scattering within the fractal aggregate. Recently, a dimensionless correction factor h has been determined to correct the aggregate absorption cross section of the RDG-FA theory based on the accurate results of DDA [8]. DDA is a numerical method consisting in decomposing the particle by a number of spatially uniformly distributed discrete dipoles. The main advantage of DDA relative to other methods is its capability of handling any shaped particles with different compositions. Accurate radiative properties of the particle can be achieved when the number of dipoles used in the decomposition is sufficiently high; however, the computing time also increases significantly with the number of dipoles. As a consequence, a judicious choice of the number of dipoles has to be made in DDA calculations. DDA has been extensively validated against results of other methods and experimental measurements [30].

The h function has been determined for many numerical aggregates (fractal dimension $D_f = 1.78$ and fractal prefactor $k_f = 1.44$) generated by a DLCA algorithm by dividing the absorption cross sections evaluated by DDA by their corresponding RDG-FA results (see Fig. 1 below). In [8], the h function has been determined for seven wavelengths between 266 and 1064 nm for a wide range of aggregate size between $N_p = 1$ and up to 1006. It is worth pointing out that in [8], the primary spheres distribution was

considered Gaussian with the mean and standard deviation being 34.2 and 6.85 nm, respectively. Unless otherwise indicated explicitly, the numerical results presented below were obtained for these DLCA aggregates.

Thus, by taking into account the effect of multiple scattering through the correction factor h , the analytical expression for the absorption coefficient of an ensemble of poly-disperse aggregates can be written as:

$$K_{\text{abs}}(\lambda) = N_{\text{tot}} \int_0^\infty C_{\text{abs}}^{\text{mono}}(\lambda) h(\lambda, N_p) N_p p(N_p) dN_p \quad (4)$$

where N_{tot} denotes the aggregate number density and $p(N_p)$ represents the probability density function of aggregate size expressed in terms of number of primary spheres per aggregate N_p . The aggregate size distribution can generally be considered as lognormal, i.e., defined by two parameters: the median diameter $N_{p,\text{geo}}$ and the geometric standard deviation σ_{geo} . Under the assumption that primary particles are much smaller than the wavelength, the Rayleigh theory can be used to express the primary particle absorption cross section as $C_{\text{abs}}^{\text{mono}} = \pi^2 D_p^3 E(m) / \lambda$.

The combination of Eqs. 3 and 4 results in the following expression for the LII signal:

$$\begin{aligned} \text{LII}(\lambda_{\text{det}}) &= \frac{\pi^2 \Delta V C_1 \eta_{\lambda_{\text{det}}} D_p^3 N_{\text{tot}}}{D^2} \underbrace{\int_0^\infty h(\lambda_{\text{det}}, N_p) N_p p(N_p) dN_p}_{\overline{N_p^*}(\lambda_{\text{det}})} \frac{E(m, \lambda_{\text{det}})}{\lambda_{\text{det}}^6} \\ &\quad \left(\exp\left(\frac{C_2}{\lambda_{\text{det}} T}\right) - 1 \right)^{-1} \Delta \lambda_{\text{det}} \end{aligned} \quad (5)$$

where $\overline{N_p^*}$ is an optically equivalent mean number of primary particle per aggregate that incorporates the multiple scattering effects. The soot particle volume fraction can then be expressed as:

$$f_v = \frac{\pi D_p^3}{6} N_{\text{tot}} \underbrace{\int_0^\infty N_p p(N_p) dN_p}_{\overline{N_p}} \quad (6)$$

where $\overline{N_p}$ is the mean number of primary particle per aggregate. The combination of Eqs. 5 and 6 leads to the following revised expression for the LII signal:

$$\begin{aligned} \text{LII} &= \frac{6\pi^2 V C_1 \eta_{\lambda_{\text{det}}}}{D^2} f_v \frac{\overline{N_p^*}(\lambda_{\text{det}})}{\overline{N_p}} \frac{E(m, \lambda_{\text{det}})}{\lambda_{\text{det}}^6} \\ &\quad \times \left(\exp\left(\frac{C_2}{\lambda_{\text{det}} T}\right) - 1 \right)^{-1} \Delta \lambda_{\text{det}} \end{aligned} \quad (7)$$

When the multiple scattering effect is neglected as a consequence of using the RDG-FA aggregate absorption

cross section, the ratio $\overline{N_p^*} / \overline{N_p}$ becomes unity and thus the revised expression for the LII signal given in Eq. 7 is then consistent with the expressions found in the literature, which indicates that the LII signal is proportional to the soot volume fraction if the particle size-dependent temperature is not explicitly accounted for. However, the present development of the multiple scattering effect on aggregate absorption, and hence emission, suggests that accounting for the aggregate morphology and the aggregate size distribution-dependent multiple scattering effects can produce a deviation from the established concept about the relation between LII signal and soot volume fraction.

To quantify the ratio $\overline{N_p^*} / \overline{N_p}$, we first need to extract the analytical expression for the correction factor h in Eqs. 4 and 7 from the results published previously [8]. For aggregates whose size is sufficiently large to exhibit a power-law behavior, the asymptotic form of the h function for large aggregates can be expressed as follows

$$\begin{aligned} h^\infty &= 1.11 \alpha_2^2 N_p^{2(\alpha_1 - 1)} \\ \alpha_1 &= \left(a + b \frac{\ln(\lambda/\lambda_0)}{\lambda/\lambda_0} \right)^{-1} \quad \text{with } a = 0.9871, \\ &\quad b = 2.4878 \quad \text{and } \lambda_0 = 1 \text{ nm.} \\ \alpha_2 &= \left(a + b \frac{\ln(\lambda/\lambda_0)}{\lambda/\lambda_0} + c \left(\frac{\lambda_0}{\lambda} \right)^{1.5} \right)^{-1} \quad \text{with} \\ &\quad a = 1.0209, \quad b = -24.0657, \quad c = 2244.37 \\ &\quad \text{and } \lambda_0 = 1 \text{ nm.} \end{aligned} \quad (8)$$

To ensure the h function also produces the correct value of unity for isolated primary particles, the h function is expressed in the following form

$$h = h^\infty + (1 - h^\infty) \exp\left(-\frac{2}{3} (N_p - 1)^{0.5}\right) \quad (9)$$

Figure 1 compares the h function values from Eq. (9) against the DDA results over a wide range of aggregate size N_p (1–1006) and wavelength (266–1064 nm). The dashed lines correspond to the correlation results given by Eqs. 8 and 9. It is evident that the correlations given in Eqs. 8 and 9 for the h function are reasonably accurate; however, discrepancies between the correlations and the DDA results exist for relatively small aggregates around $N_p = 10$.

Figure 2 displays the contours of the $\overline{N_p^*} / \overline{N_p}$ ratio as a function of the aggregate size distribution through its two parameters: modal gyration diameter $D_{g,\text{geo}}$ and geometric standard deviation $\sigma_{g,\text{geo}}$ and for three wavelengths of 266, 632, and 1064 nm. Here, the lognormal aggregate size

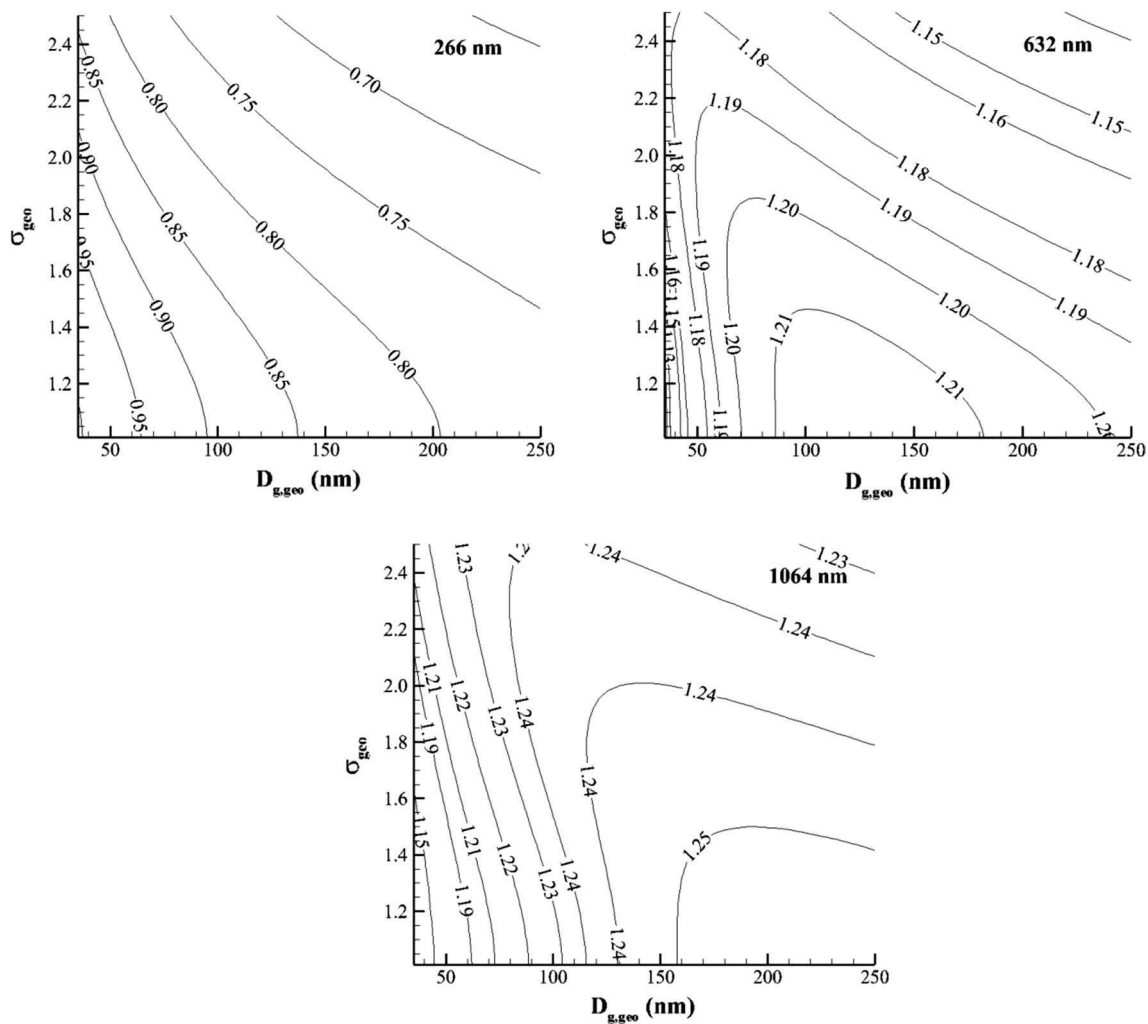


Fig. 2 Variation of the ratio $\overline{N_p^*}/\overline{N_p}$ with the lognormal aggregate size distribution expressed in the gyration diameter for three wavelengths. Conversion in gyration diameter is achieved by using the fractal law with $D_p = 34.2$ nm, $D_f = 1.78$, and $k_f = 1.44$

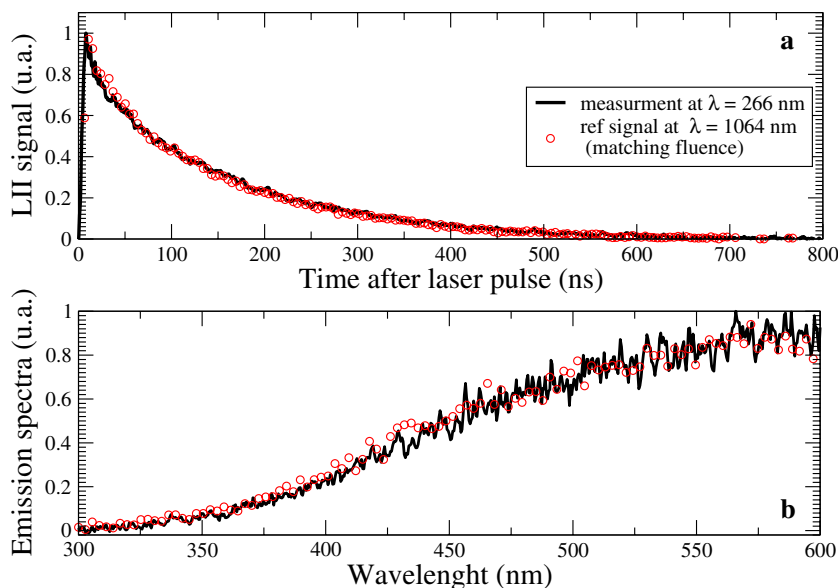
distribution is expressed in terms of the aggregate gyration diameter instead of the number of primary particles in an aggregate N_p , since the aggregate gyration diameter is an easier and more convenient parameter to interpret light scattering experiments and is often used by experimentalists. The gyration diameter is linked to the number of primary particle in an aggregate by the well-known fractal law $N_p = k_f (D_g/D_p)^{D_f}$. Note that the volume fraction determined by LII measurement without taking into account the aggregate morphology-dependent multiple scattering effect (classical approach, i.e., $\overline{N_p^*}/\overline{N_p} = 1$) has to be divided by the proposed correction factor shown in Fig. 2. Consequently, we can conclude that the classical analysis of the LII signal underestimates the actual volume fraction by about between 5 and 54 % at $\lambda_{\text{det}} = 266$ nm, overestimate the real volume fraction by 12–17 % at $\lambda_{\text{det}} = 632$ nm, and

13–19 % at $\lambda_{\text{det}} = 1064$ nm for the DLCA aggregates considered, depending on the aggregate size distribution.

In the 2C-LII technique, the soot temperature is determined by the ratio of LII signals detected at two different narrow bands in the visible spectrum [5]. Since the multiple scattering effect on aggregate absorption (hence emission) is wavelength dependent as illustrated in Fig. 1, the introduction of the wavelength-dependent correction factor to the RDG-FA expression for aggregate absorption cross section also affects the determination of soot temperature from the LII signal ratio. Such effects have been investigated previously by Liu and Smallwood [9].

The results shown in Fig. 2 suggest that the multiple scattering effect is not negligible compared to measurement uncertainties and should be taken into account to improve the accuracy of the LII technique. It is also

Fig. 3 Example of temporal (recorded at 720 ± 16 nm to avoid any LIF signal for 266-nm laser excitation) (a) and spectral (recorded at 60 ns after the laser pulse with a gate width set to 50 ns to avoid any LIF signal for 266-nm laser excitation) profiles of LII signals (b), obtained at $\lambda = 266$ nm and $\lambda = 1064$ nm for matching fluencies at 15 mm HAB in a rich premixed flat flame of $\text{CH}_4/\text{O}_2/\text{N}_2$ [1]



important to ensure that the multiple scattering effect is properly accounted for during the calibration of a LII system. For example, let us consider the calibration performed at a given position in a flame whose soot volume fraction is obtained by inversion of line-of-sight attenuation data taken at the same wavelength as the LII signal detection wavelength λ_{det} . Assuming the detection wavelength is long enough to neglect the contribution of scattering to extinction, the expression for the extinction coefficient becomes:

$$K_{\text{ext}}(\lambda_{\text{det}}) \cong K_{\text{abs}}(\lambda_{\text{det}}) = \frac{6\pi}{\lambda_{\text{det}}} \frac{\overline{N_p^*}(\lambda_{\text{det}})}{\overline{N_p}} E(m, \lambda_{\text{det}}) f_v \quad (10)$$

The term $\overline{N_p^*} / \overline{N_p}$, which is aggregate size distribution and wavelength dependent, should in general be taken into account to obtain the local soot volume fraction from Eq. (10) to be consistent with the improved expression for LII signal given in Eq. (7). It should be noted that the aggregate size distribution at the calibration point is required in Eq. (10), whereas the aggregate size distribution at the measurement point, which can be quite different from that at the calibration point, is needed in the LII signal expression given in Eq. (7). Unfortunately, knowledge of the aggregate size distribution is in general not available without performing additional experiments, such as laser scattering or soot sampling followed by transmission electron microscope (TEM) image analysis. Various methods have been proposed and applied to determine the soot refractive index or the soot absorption function variation with wavelength. A fairly simple method to infer the relative spectral variation of $E(m)$ with wavelength is based on low-fluence LII measurements using pulsed lasers of two excitation wavelengths, i.e., TEW-LII [1, 14, 31]. This method is briefly reviewed in the next section, and the

impact of multiple scattering will be incorporated into the theory of TEW-LII.

2.2 Impact of aggregate morphology on TEW-LII method: $E(m, \lambda)/E(m, 1064 \text{ nm})$

The authors of this technique [1] observed that at a given position in a flame and for the same detection $\Delta\lambda_{\text{det}}$, the amplitude, temporal decay, and spectral dependence of the LII signal could be nearly identical for different excitation wavelengths when proper laser pulse energies were selected, as illustrated in Fig. 3.

At a given location in a sooting flame when the LII signals are identical by adjusting the pulse energy of each laser, it can be concluded that the total laser energy absorbed by the particles, the peak temperature reached by the particles, and the rate of particle cooling to the surrounding gas under the excitation by these lasers should all be the same.

Thus, when LII signals produced by two different excitation laser sources at wavelengths $\lambda_{\text{exc},1}$ and $\lambda_{\text{exc},2}$ match perfectly, the total laser energy absorbed by the particles is identical

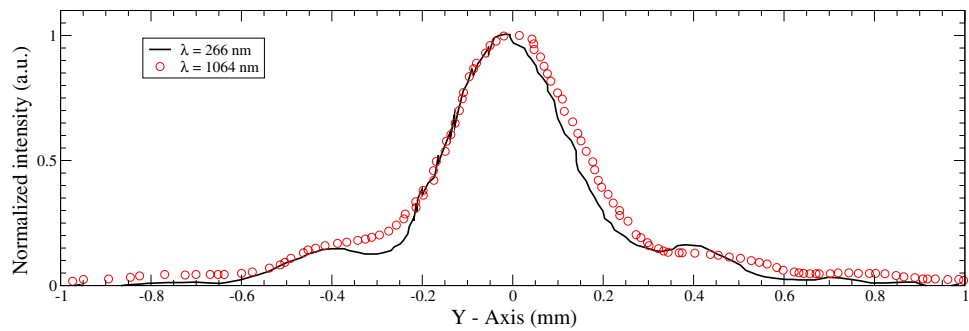
$$\int_0^{\Delta t_{\text{laser}1}} H_{\text{abs}}(\lambda_{\text{exc},1}) dt = \int_0^{\Delta t_{\text{laser}2}} H_{\text{abs}}(\lambda_{\text{exc},2}) dt \quad (11)$$

where H_{abs} represents the rate of light absorption by the particles under excitation per unit volume and Δt_{laser} the laser pulse duration. The laser energy absorption rate is dependent on the laser intensity $I_\lambda(t)$ and on the absorption coefficient K_{abs} (given in Eq. 4):

$$H_{\text{abs}}(\lambda) = I_\lambda(t) K_{\text{abs}}(\lambda) \quad (12)$$

To apply the TEW-LII method, a particular effort has to be done to obtain identical laser beam profiles as illustrated in Fig. 4. This ensures that the volume of measurement and

Fig. 4 Matching of the spatial laser profiles for Gaussian laser profiles at 266- and 1064-nm wavelengths



particle concentration are the same when two different excitation lasers are used. After some simplifications, the substitution of Eqs. 4 and 12 in Eq. 11 leads to

$$\begin{aligned} \frac{E(m, \lambda_{\text{exc},1})}{\lambda_{\text{exc},1}} \frac{\Delta t_{\text{laser}1}}{\int_0^{\Delta t_{\text{laser}1}} I_{\lambda_{\text{exc},1}}(t) dt} \int_0^{\infty} h(\lambda_{\text{exc},1}, N_p) N_p P(N_p) dN_p \\ = \frac{E(m, \lambda_{\text{exc},2})}{\lambda_{\text{exc},2}} \frac{\Delta t_{\text{laser}2}}{\int_0^{\Delta t_{\text{laser}2}} I_{\lambda_{\text{exc},2}}(t) dt} \int_0^{\infty} h(\lambda_{\text{exc},2}, N_p) N_p P(N_p) dN_p \end{aligned} \quad (13)$$

The integration of the laser pulse intensity over time corresponds to the experimentally determined laser pulse energy $e_{\lambda_{\text{exc}}}$. The second integral (over N_p) is similar to the one presented in Eq. 5 and can be written as $\overline{N_p^*}(\lambda_{\text{exc}})$. Finally, Eq. 13 becomes:

$$\frac{E(m, \lambda_{\text{exc},1})}{E(m, \lambda_{\text{exc},2})} = \frac{\lambda_{\text{exc},1} e_{\lambda_{\text{exc},2}} \overline{N_p^*}(\lambda_{\text{exc},2})}{\lambda_{\text{exc},2} e_{\lambda_{\text{exc},1}} \overline{N_p^*}(\lambda_{\text{exc},1})} \quad (14)$$

Equation (14) indicates that the relative spectral dependence of the absorption function can be determined with known laser pulse energies of the two excitation lasers when the resultant LII signals are matched. The $E(m, \lambda)/E(m, 1064 \text{ nm})$ ratio determination is based on the comparison of the total energy absorbed by the particles during the laser pulse. In this method, the $E(m, \lambda)$ and $E(m, 1064 \text{ nm})$ are considered constant over the temperature range of soot particles during the laser heating. In this case, the soot particle temperature is between the flame temperature and the LII peak temperature, which is about 3500 K because of the use of low laser energy to avoid soot sublimation. Bejaoui et al. fixed $\lambda_{\text{exc},2} = 1064 \text{ nm}$ while varying $\lambda_{\text{exc},1}$ from 266 to 660 nm [1]. Because, up to now, the aggregate morphology-dependent multiple scattering effect was not considered, the ratio $\overline{N_p^*}(\lambda_{\text{exc},2})/\overline{N_p^*}(\lambda_{\text{exc},1})$ was neglected in the determination of $E(m)$ ratio (considered equal to 1) corresponding to isolated primary spheres ($N_p = 1$). By making this approximation, Bejaoui et al. [1] found similar spectral dependence of the relative absorption function regardless of the type of fuel or the position in the flames they investigated. These findings were questioned because

some studies have shown that the absorption function varies with the level of soot maturation [11, 32, 33]. Nevertheless, the present study suggests that taking into account, the multiple scattering effects on aggregate absorption could potentially change the conclusions of Bejaoui et al. [1] when their TEW-LII results are interpreted using the expression given in Eq. (14), since $\overline{N_p^*}(\lambda_{\text{exc},2})/\overline{N_p^*}(\lambda_{\text{exc},1})$ can be different than unity, depending on the aggregate size distribution and $\lambda_{\text{exc},1}$. Indeed, Fig. 5 shows that the ratio $\overline{N_p^*}(1064 \text{ nm})/\overline{N_p^*}(\lambda_{\text{exc},1})$ is significantly greater than unity at lower wavelengths and becomes slightly higher than unity (within about 10 %) for wavelengths larger than 532 nm. The impact of these corrections on the relative $E(m)$ variation with wavelength is discussed in the next section.

3 Results and discussion

In this section, the corrections introduced above are applied to re-analyze the recent results of Bejaoui et al. [1] obtained by the TEW-LII method in a premixed methane flame at different heights above the burner (HAB). Based on a recent evaluation of the absolute values of $E(m)$ at $\lambda = 1064 \text{ nm}$ at different HAB in the same flame [34], the spectral dependence of soot absorption function values as a function of HAB is determined.

3.1 The flat premixed flame investigated

The investigated flame in this study is a flat premixed methane flame stabilized on a commercial McKenna burner operated at atmospheric pressure. The equivalence ratio was set at 2.15 by premixing methane (2.47 slpm), oxygen (2.3 slpm), and nitrogen (5.17 slpm) before the mixture was delivered to the bronze porous sintered matrix. A stabilization steel plate was placed at 20 mm above the burner exit surface, and a nitrogen flow through a co-annular porous sintered matrix was used to help stabilization of the sooting flame and prevent the formation of an outer diffusion flame. Further details of the experimental conditions to generate the flame were described in [35].

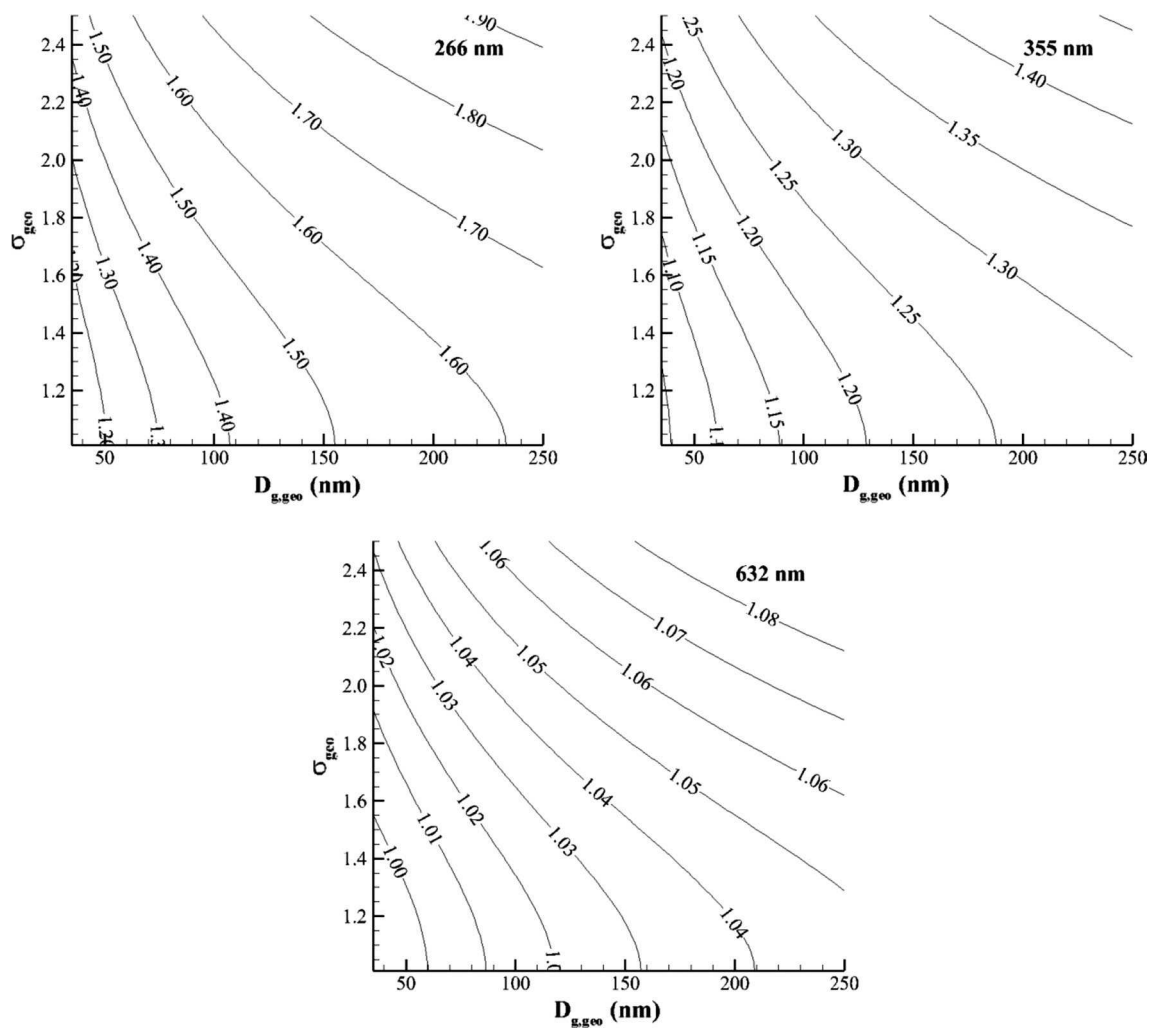


Fig. 5 Variation of $\bar{N}_p^*(1064 \text{ nm}) / \bar{N}_p^*(\lambda_{\text{exc},1})$ with the lognormal aggregate size distribution expressed in the gyration diameter for

three wavelengths $\lambda_{\text{exc},1} = 266, 355,$ and 632 nm . Conversion from the aggregate size N_p to the gyration diameter is achieved by using the fractal scaling law with $D_p = 34.2 \text{ nm}$, $D_f = 1.78$, and $k_f = 1.44$

3.2 The TEW-LII setup

The TEW-LII method has been applied to the flat premixed flame described above to investigate the relative spectral variation of $E(m)$ at several wavelengths relative to the value at 1064 nm . An example of the spectral and temporal profiles of LII signals obtained at 15 mm HAB in this flame is given in Fig. 3. The TEW-LII setup consisted of a YAG laser at 1064 nm for the reference excitation, and for other investigated wavelengths, another laser source ranging from UV to visible ($\lambda = 266, 355, 532,$ and 660 nm) was used. The system has been described previously in [1]. Briefly, 266- and 532-nm laser beams were, respectively, obtained by using the fourth harmonic and the second harmonic of a Nd:YAG. The 355-nm laser beam was generated using the frequency tripler of a Nd:YAG. The 660-nm laser beam was emitted by an optical parametric

oscillator pumped by the third harmonic of the Nd:YAG. In each pair of laser beams ($\lambda, 1064 \text{ nm}$), the laser pulse durations were adjusted (FWHM duration = 6 ns for the 266/1064 nm and 532/1064 nm, FWHM duration = 11 ns for the 355/1064 nm and 660/1064 nm pairs). The laser beams were perfectly aligned within the flame position with an identical shape (a nearly tophat spatial profile for the 355/1064 nm and 660/1064 nm pairs and an Airy diffraction profile for the 266/1064 nm and 355/1064 nm pairs, see Fig. 4).

In order to measure the ratios of laser pulse energy leading to $E(m, \lambda)/E(m, 1064 \text{ nm})$, temporally and spectrally resolved LII signals were acquired for each laser excitation configuration using the same LII detection arrangement [1]. Briefly, the time-resolved LII (TiRe-LII) measurements were taken with a photomultiplier tube (500 LII time decays averaged with a detection bandpass filter centered at

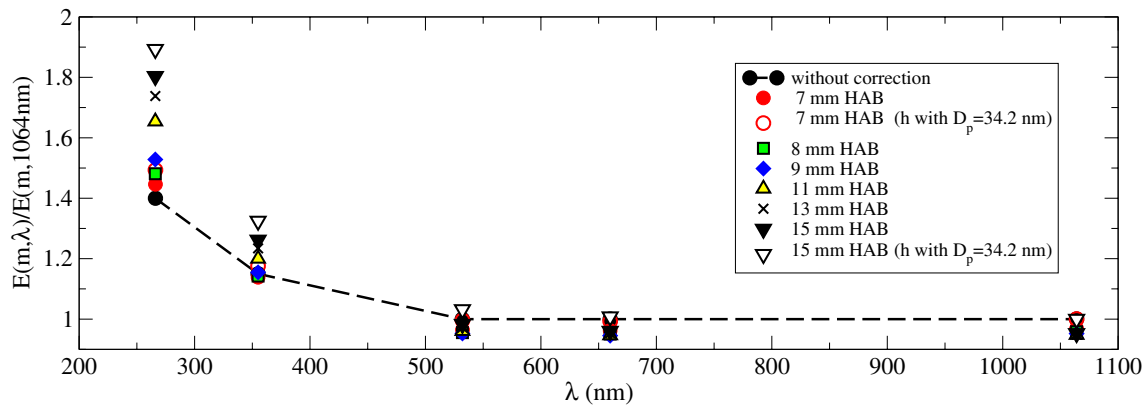


Fig. 6 Effects of the correction factor due to multiple scattering on the evaluation of the relative spectral dependence of the absorption function at different heights above the burner

720 nm to avoid any laser-induced fluorescence, LIF, signal coming from PAH and/or soot precursors in the flame at $\lambda_{\text{laser}} = 266$ nm [35]). LII spectra were obtained by means of imaging spectrograph coupled to an ICCD camera (60 ns delayed after the peak of the laser pulse with a gate width set to 50 ns to avoid LIF or any other laser-induced non-incandescence signals), with the photomultiplier tube and the camera being connected simultaneously to the two exit ports of the spectrograph.

The relative spectral dependence of $E(m)$ obtained by the TEW-LII method without taking into account the aggregate morphology and multiple scattering, i.e., setting $\overline{N}_p^*(\lambda_{\text{exc},2})/\overline{N}_p^*(\lambda_{\text{exc},1}) = 1$ in Eq. 14, is almost identical at any HAB, as reported by Bejaoui et al. [1], and plotted in Fig. 6 as black-filled circles. For example, the ratio of laser energies $e_{\text{laser}}(266 \text{ nm})/e_{\text{laser}}(1064 \text{ nm}) = 0.18$ while the laser fluence at 1064 nm is lower than soot sublimation threshold found to be around 0.2 J/cm^2 measured at $1/e^2$ of the fluence peak. The independence of the relative spectral variation of $E(m)$ with HAB has been systematically established by the same group for all investigated flames at atmospheric pressure [1]. However, this was not the case when the method was applied to a low-pressure methane/oxygen/nitrogen flame (equivalence ratio 2.32) [33]. In this case, a significant decrease in the ratio $E(m, 532 \text{ nm})/E(m, 1064 \text{ nm})$ in the soot nucleation zone was observed. Above this zone, the ratio was found to be almost constant. It should be noted that the soot concentration was very low in this low-pressure flame (around 1 ppb) and there should be very low level of soot aggregation. In consequence, the results of [33] are considered more reliable than those presented in [1] with regard to the relative spectral variation of $E(m)$, since the neglect of the term $\overline{N}_p^*(\lambda_{\text{exc},2})/\overline{N}_p^*(\lambda_{\text{exc},1})$ in Eq. 14 seems more justified. It is reasonable to state that the locations investigated in [1] are beyond the nucleation zone based on a more recent

study conducted in the same flame [34], where soot sampling followed by TEM image analysis at different heights above the burner was conducted. Nevertheless, neglect of the term $\overline{N}_p^*(\lambda_{\text{exc},2})/\overline{N}_p^*(\lambda_{\text{exc},1})$ in the analysis of [1] is questionable.

3.3 Soot sampling/TEM image analysis

For the determination of soot primary particle diameter and aggregate size distributions, soot was sampled at selected heights above the burner along the flame centerline for TEM imaging and subsequent image analysis [34]. At HAB below 9 mm, attempts to collect very young soot particles suitable for TEM image analysis were not successful, so data at HAB = 7 and 8 mm were estimated based on the trend of the lognormal parameters over the range of HAB above 9 mm [34]. TEM images of the sampled soot were analyzed for primary soot particle diameter and aggregate size distributions by Image J software. The modal primary diameter and the lognormal distribution parameters for D_p and N_p distributions at different HAB are summarized in Table 1, which are taken from the recent study of Bejaoui et al. [34].

3.4 Evaluation of absolute absorption function at 1064 nm

The value of $E(m)$ at 1064 nm as a function of HAB in the rich premixed flat methane flame has been recently determined in the study of Bejaoui et al. [34]. The principle for deriving the soot $E(m)$ value using a low-fluence LII technique has been described and demonstrated by Snelling et al. [36]. Briefly, for known laser pulse properties (wavelength, temporal, and spatial laser intensity distributions), local gas temperature, and the soot primary particle and aggregate size distributions, the value of $E(m)$ can be

Table 1 Soot aggregate size distributions (lognormal, expressed in terms of number of primary spheres) and values of the absorption function at 1064 nm at different heights above the burner exit surface (from Bejaoui et al. [34])

HAB (mm)	D_p (nm)	$N_{p,geo}$ (-)	$\sigma_{p,geo}$ (-)	$E(m, 1064 \text{ nm})$
7	8.5	1.2	1.05	0.22
8	9.0	1.5	1.05	0.25
9	9.5	2	1.1	0.29
11	9.8	4	1.15	0.32
13	10.0	6	1.15	0.33
15	10.3	8	1.15	0.37

determined by matching the modeled peak soot temperature to that of the measured one by two-color LII in the low-fluence regime. Further details on the determination of soot $E(m)$ at 1064 nm in the flame investigated here can be found in [34]. The $E(m)$ values at 1064 nm at different HABs are also reported in Table 1. It shows an increase in $E(m)$ at 1064 nm with increasing HAB in accordance with the results of an earlier study conducted by Bladh et al. [11]. It is worth pointing out these $E(m)$ values at 1064 nm should not be considered as accurate due to the use of density and heat capacity for mature soot, due to the unavailability of such thermal properties for young and immature soot, used in the determination of $E(m)$ values in the growth region of the flat rich premixed methane flame.

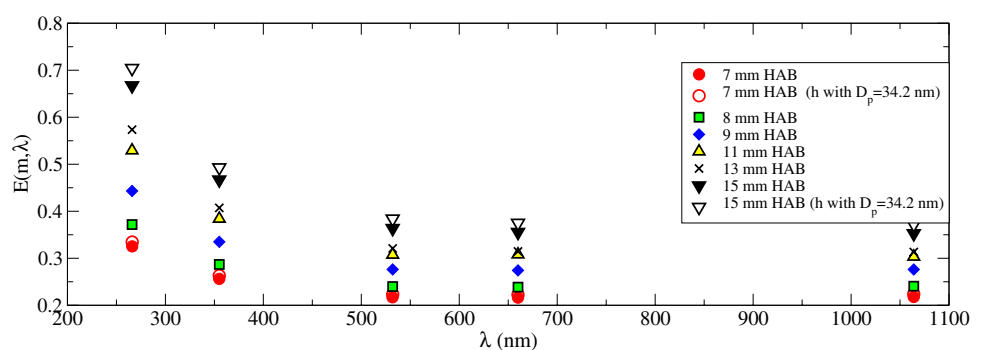
3.5 Application of the correction factors to analyze the data of Bejaoui et al. [1]

Based on the soot aggregate size distribution parameters reported in Table 1, the ratio $\bar{N}_p^*(1064 \text{ nm})/\bar{N}_p^*(\lambda_{exc})$ in Eq. 14 has been determined at different HAB and for different wavelengths. These correction factors have been used to re-analyze the experimental results of Bejaoui et al. [1] for the spectral dependence of the relative absorption function as a function of HAB. The present results with the multiple scattering effects taken into account are compared with those of Bejaoui et al. [1] (black-filled

circles) in Fig. 6. It is worth pointing out that the h functions shown in Fig. 1 and evaluated using Eqs. (8) and (9) were obtained from DDA calculations for aggregates formed by polydisperse primary particles with a diameter of 34 nm, which is much larger than the primary particle diameters in the experiments of Bejaoui et al. [1], as shown in Table 1. It is expected that decreasing the primary sphere size will reduce the multiple scattering effects and consequently makes h closer to unity. In respect of the scale invariance rule [37] and by extrapolating fitting procedure given in Eqs. 8 and 9 to longer wavelengths, such a correction becomes possible (see Appendix). In Figs. 6 and 7, we report the corrections to the evaluation of respective relative and absolute dimensionless absorption function by considering the primary particle diameters reported in Table 1. At the lowest and highest locations investigated, the derived values of $E(m, \lambda)/E(m, 1064 \text{ nm})$ and $E(m, \lambda)$ without using the scale invariance rule, i.e., by considering $D_p = 34 \text{ nm}$ in the evaluation of the h function, are also plotted in these figures to illustrate the effect of accounting for the primary particle diameter on the results.

Figure 6 shows that at a given wavelength, the absorption function ratio increases with increasing HAB. Therefore, the present results suggest that the absorption function ratio increases with increasing soot maturity, which is in contrast with the finding of López-Yglesias et al. [13], who found that the absorption cross-sectional ratio, $\sigma_{abs}(532 \text{ nm})/\sigma_{abs}(1064 \text{ nm})$, increases with decreasing soot maturity (related to the hydrogen content) in their study conducted in laminar co-flow diffusion flames. Although it is not completely clear about the causes of this qualitative difference between this study and that of López-Yglesias et al. [13] with regard to the trend of soot absorption function ratio variation with soot maturity, there are at least two plausible explanations. One lies in the different theoretical relationship between $E(m)$ and wavelength in the study of López-Yglesias et al. [13], where $E(m)$ was assumed to be proportional to wavelength λ raised to a power of $(1 - \xi)$ with ξ being a function of soot maturity and having a value around unity (about 0.8–1.3). The other is that the two investigated flames (premixed in the present

Fig. 7 Variation of $E(m)$ with wavelength at different heights above the burner exit surface with the effect of multiple scattering taken into account



study and diffusion in the study of López-Yglesias et al.) are likely to present different spatial structuration in terms of chemical structures mapping (localization of PAH's, soot precursors, and soot). This kind of differences has been put in evidence by using laser-induced fluorescence excited from UV to visible [35].

As shown in Fig. 6, the corrections due to multiple scattering effects (associated with soot aggregation) are important for wavelengths lower than 532 nm, i.e., in the near-UV spectrum, but become negligible at longer wavelengths. The influence of this correction is significant in the near-UV spectrum even though soot aggregation is not very significant throughout the premixed flame investigated as shown in Table 1. The correction to the multiple scattering effects in diffusion flames, where soot aggregation is more significant, can potentially be even more significant. We also observe in Fig. 6 that the $E(m)$ ratio is not significantly affected by the consideration of the dependence of the h function on the primary particle diameter at both heights investigated (7 and 15 mm). This is due to the fact that the corrections proposed here depend on the ratio $\overline{N}_p^*(1064 \text{ nm}) / \overline{N}_p^*(\lambda_{\text{exc}})$. Indeed, a change in h due to variation in height gives rise to a similar change in both the numerator and the denominator.

Based on the recent study of Bejaoui et al. [34], who obtained the absolute values of $E(m)$ at 1064 nm at different HABs between 7 and 15 mm in the same rich premixed methane flame as shown in Table 1, the relative variation of $E(m)$ with wavelength presented in Fig. 6 can be used to obtain the $E(m)$ values at other wavelengths.

Figure 7 presents the spectral dependence of the values of soot absorption function at different wavelengths from 266 to 1064 nm and at different HABs between 7 and 15 mm in the rich premixed flat flame of $\text{CH}_4/\text{O}_2/\text{N}_2$ investigated previously by Bejaoui et al. [34]. It is shown that the soot absorption function varies significantly with HAB in the near-UV region. For example, at 266 nm, the $E(m)$ function varies by more than a factor of 2 from 0.33 at HAB = 7 mm to 0.7 at HAB = 15 mm. Those high values of the absorption function are in accordance with previous results found in the literature. Dalzell and Sarofim [16], Chang and Charalampopoulos [38], and Lee and Tien [39] have determined soot $E(m)$ values at such low wavelengths. The significant increase in $E(m)$ with HAB in the UV spectrum is found to be driven by aggregation process (the influence of the primary particle diameter considered for the evaluation of the h function is weak) and may be explained by a reorganization of the internal microstructure moving from an amorphous internal structure to a more graphitized one. It could also be correlated with a change of hydrogen content with the soot maturity (amount of organic carbon). This interpretation needs to be confirmed by additional studies in which an analysis of the

soot internal microstructure could be conducted in the same flame so more reliable causes on the origin of the variation of the absorption function with height can be elucidated.

Finally, it should be pointed out the $E(m)$ values determined in this study should be treated with caution due to the uncertainty of the $E(m)$ values at 1064 nm determined in [34]. The significance of this study is to present a technique of how to obtain the absolute $E(m)$ values at different wavelengths by combining TEW-LII with other method which can obtain the $E(m)$ values at a specific wavelength.

4 Conclusions

The effects of multiple scattering on soot aggregate absorption and emission cross sections were incorporated into the expression for LII signal. Accounting for such effects requires the knowledge of soot fractal aggregate morphology. An analytical expression for the correction factor was proposed and shown to be reasonably accurate compared to numerical results of discrete-dipole approximation. The improved LII signal expression affects the determination of soot volume fraction and the theoretical basis of the TEW-LII technique for inferring the spectral variation of the relative soot absorption function. By this approach, LII signal is not strictly proportional to the soot volume fraction even without considering particle size-dependent soot temperature, but corrected by a factor depending on soot morphology and the detection wavelength. The present development has implications to the calibration and application of the LII techniques, as well as the determination of soot temperature using two-color LII. The effects of multiple scattering on soot aggregate absorption and emission were shown to be significant over the entire spectral range studied from 266 to 1064 nm.

The improved LII signal expression was used to re-analyze the recent experimental data of Bejaoui et al. [1]. The present results indicate that $E(m, \lambda)/E(m, 1064 \text{ nm})$ displays increasingly more significant flame location dependence with decreasing wavelength, especially at near UV below 532 nm. The present results yielded higher $E(m)$ ratios with increasing height above the burner in the investigated flame, which suggest that the $E(m)$ ratio increases with increasing soot maturity. Finally, the proposed corrections have been applied to the evaluation of the absolute $E(m)$ value at different wavelengths and at different heights above the burner in a flat premixed methane flame of Bejaoui et al. [34]. A large increase in the absorption function at 266 nm from 0.33 at HAB = 7 mm to 0.7 at HAB = 15 mm was demonstrated. Such a significant increase can be related to both an internal graphitization and by a change of composition including modification of the chemical functionality. It should be pointed out that the

$E(m)$ values presented in this study should be treated with caution since the $E(m)$ values at 1064 nm determined in [34] are subject to uncertainties.

Although the effect of scale invariance rule [37] allows the h correction function to be calculated at any primary particle diameter other than the one used its development, it does not permit wavelength-dependent $E(m)$ and can involve extrapolation to wavelengths significantly outside the range for the development of the h function. Further studies are needed to investigate how primary particle size affects the correction function to the aggregate absorption cross section and to understand the causes for the different findings between this study and that of López-Yglesias et al. [13]. It is also important to further investigate soot $E(m)$ values in different flames to gain better understanding of the relationship between soot $E(m)$ values and soot maturity.

Acknowledgments This work was conducted within the framework of French Carnot Institute Energy and Propulsion Systems (ESP). This work was also supported by the Air Quality Program of IRENI. The authors thank the CRIHAN for the computational resources provided by the Haute-Normandie region, the TEM national facility in Lille supported by CNRS (INSU), the Conseil Regional du Nord-Pas de Calais and Haute-Normandie regions, the European Funds for Regional Economic Development and the CERLA for their financial support, and the French National Research Agency (contract ANR-10-LABX-005). Fengshan Liu would like to thank the financial support by NRCan PERD AFTER Project C23.006.

Appendix 1

In this appendix, we will show that the h function determined in [8] based on DDA calculations for DLCA aggregates formed by polydisperse primary particles with a mean diameter of 34 nm can also be used to calculate the h function at any other primary particle diameters. The theoretical basis that this can be done is the scale invariance rule (SIR) demonstrated by Mishchenko [37]. SIR stipulates that the dimensionless scattering characteristics of the objects are not changed if size parameter (here $x_p = \frac{2\pi R_g}{\lambda}$) is kept constant under the assumption of a constant optical index.

More precisely, the product of the square of the wave number $k = 2\pi/\lambda$ and the particle absorption cross section (Eq. 4) is only a function of the size parameter, i.e.,

$$\frac{4\pi^2}{\lambda^2} N_p C_{\text{abs}}^{\text{mono}}(\lambda) h(\lambda, N_p, D_p) = f(x_p) \tag{15}$$

Let us now consider a reference aggregate consisting of $N_{p,\text{ref}}$ primary spheres, whose mean diameter is $D_{p,\text{ref}}$ and the corresponding gyration radius is $R_{g,\text{ref}}$. The h function of this reference aggregate has been determined at wavelength λ_{ref} . We also consider a second aggregate consisting of N_p primary particles with a mean diameter D_p .

The second aggregate can be considered as a spatially dilated version of the reference aggregate by a factor α . It is noticed that dilatation does not affect the fractal parameters. Moreover, D_p and R_g are related to the reference values as $D_p = \alpha D_{p,\text{ref}}$ and $R_g = \alpha R_{g,\text{ref}}$ [25]. We now consider the h function for the second aggregate at a specific wavelength λ which yields the same size parameter as the reference one, i.e., $D_p/\lambda = D_{p,\text{ref}}/\lambda_{\text{ref}}$. By applying SIR to the aggregate absorption cross section, one obtains

$$\begin{aligned} & \frac{4\pi^2}{\lambda_{\text{ref}}^2} N_{p,\text{ref}} \frac{4\pi x_{p,\text{ref}}^3}{k_{\text{ref}}^2} E(m, \lambda_{\text{ref}}) h(\lambda_{\text{ref}}, N_{p,\text{ref}}, D_{p,\text{ref}}) \\ &= \frac{4\pi^2}{\lambda^2} N_p \frac{4\pi x_p^3}{k^2} E(m, \lambda) h(\lambda, N_p, D_p) \end{aligned} \tag{16}$$

After simplifications, Eq. (16) becomes

$$h(\lambda, N_p, D_p) = \frac{E(m, \lambda_{\text{ref}})}{E(m, \lambda)} h\left(\lambda \frac{D_{p,\text{ref}}}{D_p}, N_p, D_{p,\text{ref}}\right) \tag{17}$$

To be consistent with the hypothesis of the SIR theorem, the refractive index, and therefore $E(m)$, is considered wavelength independent. Consequently, the h function for an aggregate consisting of $N_{p,\text{ref}}$ spheres with a mean primary particle diameter D_p at wavelength λ can be determined by using the following expression, i.e., by using the database obtained for the reference primary particle, but at a scaled wavelength of $\lambda D_{p,\text{ref}}/D_p$, i.e.,

$$h(\lambda, N_p, D_p) = h\left(\lambda \frac{D_{p,\text{ref}}}{D_p}, N_p, D_{p,\text{ref}}\right) \tag{18}$$

For the evaluation of the h function at any wavelength and for an arbitrary D_p in [8], the mean reference primary particle diameter was fixed at 34 nm. The application of SIR for the evaluation of the h function for primary particle diameters different from the reference value ($D_{p,\text{ref}} = 34$ nm) suffers two drawbacks. First, the wavelength-dependent soot absorption function cannot be taken into account. Second, application of Eq. (18) can involve extrapolation to wavelengths substantially outside the range under which the h function expressions were developed. Such extrapolation could cause error to the h function.

References

1. S. Bejaoui, R. Lemaire, P. Desgroux, E. Therssen, Appl. Phys. B Lasers Opt. **116**, 313 (2014)
2. R.W. Weeks, W.W. Duley, J. Appl. Phys. **45**, 4661 (1974)
3. A.C. Eckbreth, J. Appl. Phys. **48**, 4473 (1977)
4. L.A. Melton, Appl. Opt. **23**, 2201 (1984)
5. D.R. Snelling, G.J. Smallwood, F. Liu, Ö.L. Gülder, W.D. Bachalo, Appl. Opt. **44**, 6773 (2005)
6. C. Schulz, B.F. Kock, M. Hofmann, H. Michelsen, S. Will, B. Bougie, R. Suntz, G. Smallwood, Appl. Phys. B Lasers Opt. **83**, 333 (2006)

7. J. Reimann, S.A. Kuhlmann, S. Will, *Appl. Phys. B Lasers Opt.* **96**, 583 (2009)
8. J. Yon, F. Liu, A. Bescond, C. Caumont-Prim, C. Rozé, F.X. Ouf, A. Coppalle, *J. Quant. Spectrosc. Radiat. Transf.* **133**, 374 (2014)
9. F. Liu, G.J. Smallwood, *J. Quant. Spectrosc. Radiat. Transf.* **111**, 302 (2010)
10. R.A. Dobbins, C.M. Megaridis, *Appl. Opt.* **30**, 4747 (1991)
11. H. Bladh, J. Johnsson, N.E. Olofsson, A. Bohlin, P.E. Bengtsson, *Proc. Comb. Inst.* **33**, 641 (2011)
12. T.T. Charalampopoulos, *Rev. Sci. Instrum.* **58**, 1638 (1987)
13. X. López-Yglesias, P.E. Schrader, H.A. Michelsen, *J. Aerosol Sci.* **75**, 43 (2014)
14. J. Yon, R. Lemaire, E. Therssen, P. Desgroux, A. Coppalle, K. Ren, *Appl. Phys. B Lasers Opt.* **104**, 253 (2011)
15. E.A. Taft, H. Philipp, *Phys. Rev.* **138**, A197 (1965)
16. W.H. Dalzell, A.F. Sarofim, *J. Heat Trans.-T ASME* **91**, 100 (1969)
17. B. Vaglieco, F. Beretta, A. d'Alessio, *Combust. Flame* **79**, 259 (1990)
18. M.Y. Choi, G.W. Mulholland, A. Hamins, T. Kashiwagi, *Combust. Flame* **102**, 161 (1995)
19. S. Krishnan, K.C. Lin, G. Faeth, *J. Heat Transf.* **122**, 517 (2000)
20. R.W. Bergstrom, P.B. Russell, P. Hignett, *J. Atmos. Sci.* **59**, 567 (2002)
21. T.C. Bond, R.W. Bergstrom, *Aerosol Sci. Technol.* **40**, 27 (2006)
22. A. Coderre, K. Thomson, D. Snelling, M. Johnson, *Appl. Phys. B Lasers Opt.* **104**, 175 (2011)
23. U. Köylü, G. Faeth, *J. Heat Trans.-T ASME* **115**(2), 409–417 (1993) doi:[10.1115/1.2910693](https://doi.org/10.1115/1.2910693)
24. C. Sorensen, *Aerosol Sci. Technol.* **35**, 648 (2001)
25. J. Yon, C. Roze, T. Girasole, A. Coppalle, L. Mees, *Part. Part. Syst. Char.* **25**, 54 (2008)
26. T. Farias, Ü.Ö. Köylü, M. Carvalho, *Appl. Opt.* **35**, 6560 (1996)
27. R.K. Chakrabarty et al., *Appl. Opt.* **46**, 6990 (2007)
28. Ü.Ö. Köylü, G.M. Faeth, *J. Heat Transf.* **116**, 152 (1994)
29. G. Wang, C.M. Sorensen, *Appl. Opt.* **41**, 4645 (2002)
30. P. Sabouroux, B. Stout, J.M. Geffrin, C. Eyraud, I. Ayranci, R. Vaillon, N. Selçuk, *J. Quant. Spectrosc. Radiat. Transf.* **103**, 156 (2007)
31. E. Therssen, Y. Bouvier, C. Schoemaeker-Moreau, X. Mercier, P. Desgroux, M. Ziskind, C. Focsa, *Appl. Phys. B Lasers Opt.* **89**, 417 (2007)
32. H.A. Michelsen, P.E. Schrader, F. Goulay, *Carbon* **48**, 2175 (2010)
33. G. Cléon, T. Amodeo, A. Faccineto, P. Desgroux, *Appl. Phys. B Lasers Opt.*, 1, 297–305 (2011)
34. S. Bejaoui, S. Batut, E. Therssen, N. Lamoureux, P. Desgroux, F. Liu, *Appl. Phys. B* **118**, 449–469 (2015)
35. S. Bejaoui, X. Mercier, P. Desgroux, E. Therssen, *Combust. Flame* **161**, 2479 (2014)
36. D.R. Snelling, F. Liu, G.J. Smallwood, Ö.L. Gülder, *Combust. Flame* **136**, 180 (2004)
37. M.I. Mishchenko, *J. Quant. Spectrosc. Radiat. Transf.* **101**, 411 (2006)
38. H. Chang, T. Charalampopoulos, *Proc. R. Soc. Lond. A* **430**, 577 (1990)
39. S. Lee and C. Tien, in *Symposium (International) on Combustion* (Elsevier, 1981), pp. 1159